Studies of the Thermophysical Properties of Commercial CMSX-4 Alloy†

Taishi Matsushita,*‡ Hans-Jörg Fecht,§ Rainer K. Wunderlich,§ Ivan Egry,|| and Seshadri Seetharaman‡

Royal Institute of Technology, Sweden, Brinellvägen 23, Stockholm, SE 10044, Sweden, University of Ulm, Albert-Einstein-Allee 47, Ulm, DE 89081, Germany, and Deutsches Zentrum für Luft- und Raumfahrt, Linder Hoehe, Cologne, Delaware 51147, Germany

In this paper, measurements of the heat capacities and thermal diffusivities of commercial CMSX-4 nickel-based superalloy are described, and the results are presented. Since the as-received commercial alloy sample is not at the thermodynamic equilibrium state, the phases present in the alloy undergo transformations toward equilibrium state as the measurements are made at temperatures above which the rate of transformation can be significant. The microstructures of the as-received sample as well as heat treated samples were observed, and the relation with the properties was discussed. The results are discussed considering the phase changes occurring with the thermodynamic equilibrium state as the reference. The results are of great relevance in the performance of these alloys in industrial applications.

1. Introduction

Thermophysical properties such as thermal diffusivity and heat capacity have both theoretical as well as practical importance. In many engineering situations, it is necessary to have heat transfer data to calculate the ability of a structural component to conduct heat or to dissipate a large quantity of locally generated heat.[1] Thermal conductivities are also of fundamental interest as the mechanism of heat conduction is a structure-related phenomenon.

In recent years, mathematical modeling of the heat and mass transfer has proved to be a valuable tool in designing heat resistance materials such as Ni-base and Ti-base alloys. Thermophysical property data such as density, enthalpy, heat capacity, thermal conductivity, and thermal diffusivity are required for heat transfer computations in various processes and applications.[2] The aim of the present study is to measure the thermal diffusivities of CMSX-4 alloy in the solid state from room temperature to 1620 K using a laser flash technique. The measurements were supplemented by DSC measurements with a view to correlate the properties. The as-received as well as postmeasurement samples were examined in a scanning electron microscope to ascertain the phases present. This work has been performed as part of the ESA (European Space Agency) project, "THERMOLAB", for precision measurement of thermophysical properties of industrial alloys with a goal to optimize industrial process design and product quality.

2. Experimental

Methods for measuring the thermal diffusivity can be classified into two main groups, viz., periodic and nonperiodic heat flow methods. The periodic methods include the Ångström, thermoelectric, and radial wave methods, while nonperiodic methods include the bar, small area, semi-infinite plate, radial heat flow high intensity arc, electrically heated rod, and flash methods.[3] Most of these methods have inherent limitations due primarily to heat transport via convection as well as heat losses by radiation. The impact of these factors is minimized by the use of the laser flash technique due to the small thickness of the sample and the high-speed heat supply to the specimen.[4] The heat capacities were measured using a differential scanning calorimeter (DSC).

2.1. Materials. The nickel-based superalloy CMSX-4 was supplied by DONCASTERS (Germany) to the ThermoLab group. The composition of the alloy, presented in Table 1, was supplied by the manufacturers.

The sample was cut to the required size, and the surfaces were prepared for the thermal diffusivity measurements. Since the alloy is extremely susceptible to oxidation, both the thermal diffusivity as well as the specific heat measurements were carried out in the protective inert atmosphere of argon. The argon gas used was of Scientific 6.0 grade (99.9999 %) supplied by AGA Gas, Sweden. The gas was further purified by an elaborate gas-cleaning system to remove the traces of moisture, CO_2, and oxygen impurities. The gas purification train used is described in detail elsewhere.[5] The oxygen partial pressure of the outgoing argon gas from the measurement chamber was constantly monitored by an oxygen concentration cell with zirconia−magnesia solid electrolyte and a slow stream of dry air as the reference electrode. With the purification steps adopted, the oxygen partial pressure in the gas stream was found to be less than 10^{-15} Pa. The results of experiments where the oxygen partial pressure in the gas phase was higher were rejected.

2.2. Experimental Procedure. The details of the experimental methods are described elsewhere.[5,6] To orient the reader, only a brief description of the instruments used and the procedure adopted is presented.

A Sinku-Riko laser-flash unit (model TC-7000H/MELT) was used for the present thermal diffusivity measurements. A sapphire crucible, which is transparent to the laser beam and infrared radiation, was used as the sample holder. In the present study, the sample was prepared by polishing the surfaces. The parallelism of the surfaces was ensured by measuring the sample thickness at a number of places. In general, the sample was heated to 1573 K and cooled to room temperature at the rate of

* Corresponding author. E-mail: taishi@kth.se.
† Part of the "William A. Wakeham Festschrift".
‡ Royal Institute of Technology.
§ University of Ulm.
|| Deutsches Zentrum für Luftund Raumfahrt.

10.1021/je900132m CCC: $40.75
Published on Web 04/07/2009

Table 1. Composition of the CMSX-4 Alloy, in Mass %

Ni	Co	Cr	Ta	W	Al	Re	Ti	Mo	Si	Mn	Hf	Fe	C	Cu
balance	9.6	6.4	6.5	6.4	5.61	2.9	1.02	0.61	0.4	0.1	0.1	0.042	0.0037	< 0.001

6 K·min^{-1}. At each temperature, the sample was kept for at least 20 min to ensure that the sample had attained thermal equilibrium. The measurements were carried out by repeating the laser shots at least five times.

In the present study, the heat capacities were measured using a Netzsch STA 449C Jupiter unit. Samples were placed in a platinum crucible (inner diameter of 6 mm and a height of 4 mm) with sapphire linear. A platinum lid was placed on top. The sapphire linear was tight-fitted to the platinum crucible to reduce the risk of heat loss by radiation. The sample was heated at different heating rates, i.e., (2, 5, 10, and 20) K·min^{-1}, and then cooled to 293 K at the same rate.

In both thermal diffusivity and specific heat measurements, the sample was protected by purified Ar gas (Partial oxygen pressure, $Po_2 < 10^{-15}$ atm).

3. Results and Discussion

3.1. Phase Diagram of CMSX-4. A phase diagram of an alloy which is close to that of the CMSX-4 nickel base superalloy used in the present studies was computed by the use of the TCNI1 database available with the Thermo-Calc software (ver. Q), for the temperature interval (600 to 2000) K. In the calculation, the following major components were used for the calculation, i.e., Ni, Co, Cr, W, Al, Re, and Ti. Tantalum was excluded as it has not yet been assessed in the database. A plot of the composition of the various phases existing at different temperatures according to the above computation is presented in Figure 1.

From the calculated phase diagram, it was found that the ordered γ' (Ni_3Al) phase would dissolve gradually into the γ phase over a wide temperature range, and there is no first-order transition except for the melting process. According to the calculation, the solidus and liquidus temperatures were (1655 and 1680) K, respectively. Once again, one of the main compositions Ta was excluded in the calculation as it is not assessed in the database. This fact will give error for the temperatures. Further, the 0.0037 % C was ignored. Therefore, carbide formation, including TaC, is not assessed.

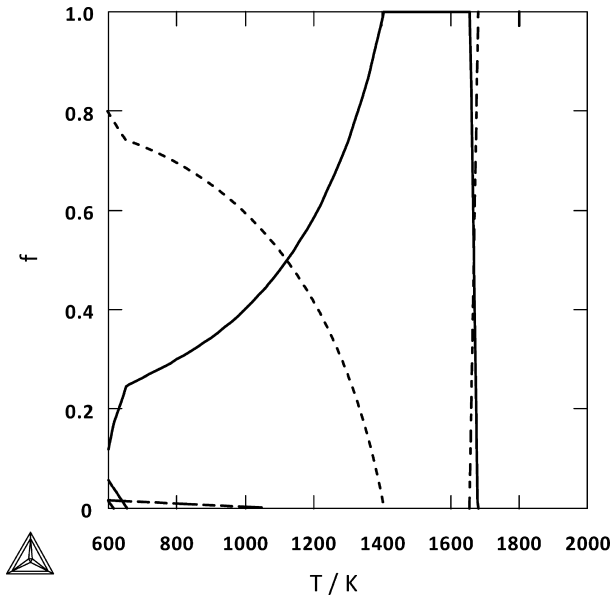

Figure 1. Temperature plotted against the composition of the individual phases (fraction, f) identified to exist in the alloy in the temperature interval (600 to 2000) K. Software, Thermo-Calc (Ver. Q); Database, TCNI1, $P = 10^5$ Pa, N (Total mole) = 1. Composition: Ni, Co, Cr, W, Al, Re, and Ti as in Table 1. —, γ phase; — - — - —, liquid; - - -, γ' phase; and — — —, σ phase.

3.2. Microstructure of the CMSX-4.[5] Scanning electron microscope (SEM) studies of the as-received samples as well as those heat-treated were carried out and compared with the phase relationships presented in Figure 2. While a number of alloy samples were heat-treated and quenched for mapping the phases present, only three important results are presented here. Figure 2 shows the SEM images of the microstructure of the samples:

(a) as-received sample;

(b) heated to 1000 at 6 K·min^{-1} and quenched,

(c) heated to 1573 K and cooled to 1000 at 6 K·min^{-1} and quenched.

It can be seen in Figure 2(a) that the size and shape of the cubic γ' phase are small and regular in the as-received sample. The structure does not exhibit a significant change (Figure 2(b)) as the sample is heated to 1000 at 6 K·min^{-1} and quenched indicating thereby that the dissolution of the γ' phase has not occurred to a significant extent. However, following the complete dissolution of the γ' phase at high temperature (1573 K) and cooling to 1000 K, the γ' phase is reprecipitated. It can also be seen that the grains of the γ' phase have coarsened, and the shape of these grains is irregular (Figure 2(c)).

3.3. Thermal Diffusivity of the CMSX-4. In the present work, the thermal diffusivity of the CMSX-4 alloy in the as-received condition was measured as a function of temperature[5]

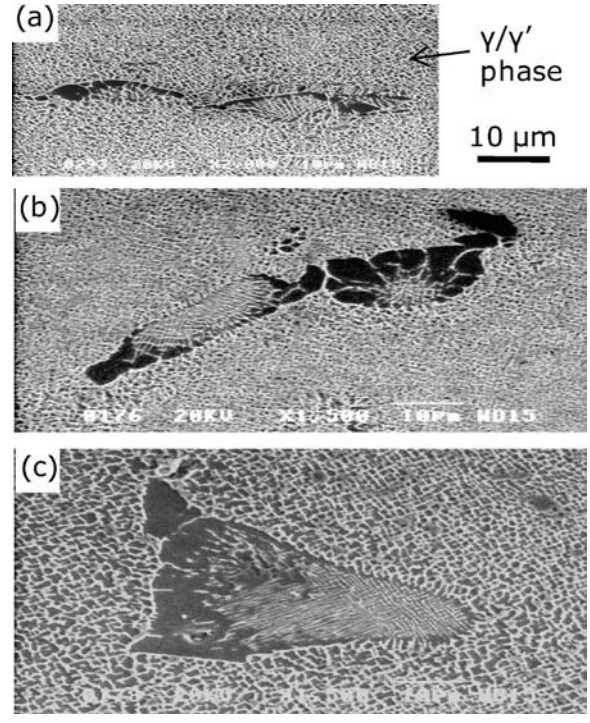

Figure 2. SEM images of the microstructure of CMSX-4. White part: γ phase; gray part, γ' phase. (a) As-received sample, (b) heated to 1000 K at 6 K·min^{-1} and quenched, and (c) heated to 1573 K and cooled to 1000 K at 6 K·min^{-1} and quenched.

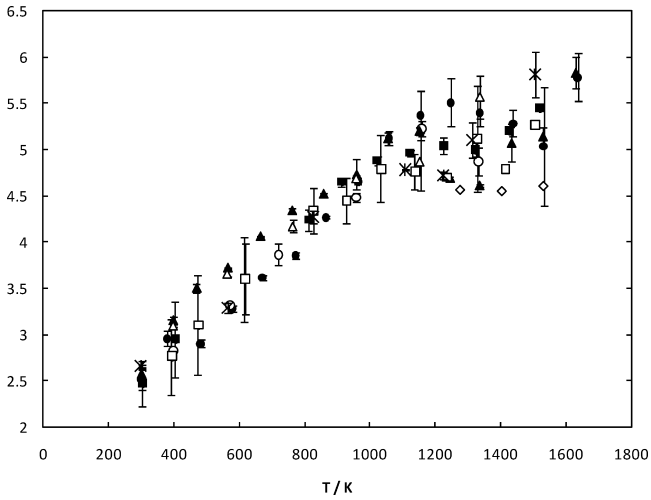

Figure 3. Thermal diffusivity, $\alpha/10^{-6}\cdot m^2\cdot s^{-1}$, of the CMSX-4 as a function of temperature, T/K.[5] ●, Heating 1; ○, Cooling 2; ▲, Heating 2; △, Cooling 2; ■, Heating 3; □, Cooling 3; *, Heating 4; and ◇, Cooling 5.

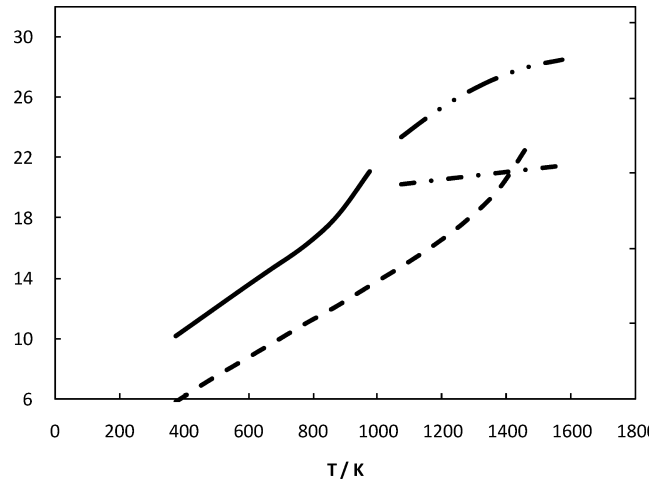

Figure 4. Thermal conductivity, $\lambda/W\cdot m^{-1}\cdot K^{-1}$, of the CMSX-4 as a function of temperature, T/K. - - -, Wiedemann−Franz law; —, $c_p\cdot\rho\cdot\alpha$; — - - —, $c_p\cdot\rho\cdot\alpha$ (max estimation of α); and — - —, $c_p\cdot\rho\cdot\alpha$ (min estimation of α).

with the aid of the laser flash method. The sample was heated and cooled at 6 $K\cdot min^{-1}$, and the thermal diffusivity was measured in both heating and cooling cycles. The sample was soaked at least 20 min at each experimental temperature to get thermal equilibrium. The details of the experimental method are described elsewhere.[5] The results of the measurements are reproduced in Figure 3. The treatment of the sample for "Cooling 5" in the figure was different from the others. The sample was heated to 1573 K and kept for 12 h and brought down to lower temperatures.

It is seen in Figure 3 that the thermal diffusivity of the as-received alloy shows an increase in the range room temperature to ca. 1200 K. This increase may be attributed to a number of factors. The sample that was heat treated at 1573 K for 12 h and then cooled (sample 5 in Figure 3) shows thermal diffusivities in the cooling mode which are in agreement with the nonequilibrium samples indicating that the increase cannot be attributed to the dissolution of the γ' phase. Similar behavior has been noticed in a number of other alloys studied in the present division. Thermal diffusivity is found to show a slight decrease in each individual run at higher temperature range and increased again. Considering the experimental scatter in the temperature range (200 to 1000) K, it is seen in Figure 3 that the scatter is increased at higher temperatures. This may be due to the experimental factor that the I.R. detection in the instrument has been optimized for the high-temperature measurements, especially for the temperature range of (1073 to 1473) K. On the other hand, in the temperature range (1100 to 1550) K, the scatter of the thermal diffusivity values (maximum scattering about ± 15 %) between the measurements with different samples was more significant at high temperatures.

As can be seen from the calculated phase diagram (Figure 1), the γ' phase dissolves continuously into the γ phase over a wide temperature range. However, the change of the γ/γ' ratio becomes much steeper in the higher temperature range (about 1300 K to solvus temperature of the γ' phase). This drastic phase change leads to an increasing of disorder of the phases as the γ' dissolution takes place resulting in a constant to near-decreasing trend in the thermal diffusivities.

It is seen in Figure 3 that the thermal diffusivity values show a significant scatter in this temperature range. It is to be noted that during the measurements the sample is soaked at each of the experimental temperatures for at least 20 min. It is likely that the ratio of the γ/γ' phases would change during the measurements. Thus, the degree of the disorder is also not constant during the measurement at fixed temperature. This phase change would also lead to scattering the measurement values. From these facts, it can be concluded that the thermal diffusivity values are strongly dependent on the ratio of the γ/γ' phases and the degree of disorder in the phases.

In general, in thermal diffusivity measurements of the nonequilibrium, alloys may be expected to exhibit a hysteresis between the heating and cooling cycles of the same sample, as there is likely to be coarsening of the grains. Increase in grain size should lead to an increase in the thermal diffusivities. It is seen in Figure 3 that the results obtained during heating and cooling cycles for the various samples are close to each other. It is particularly interesting to examine the results for the cooling of sample 5, which has been kept at 1573 K for 12 h before the measurements were made in the cooling mode. These results are close to the values obtained for other samples in the heating and cooling modes. The coarsening of the grains must be significant in this case as can be seen in the case of the alloy heated to 1573 K followed by cooling to 1000 K and subsequent quenching (Figure 2(c)) which has resulted in significantly coarser grains. On the other hand, in Figure 3, the results corresponding to the cooling of sample 5 are not significantly different from the others. Thus, the present results indicate that the impact of coarsening of the grains may not be significant.

The thermal conductivity, λ, of the CMSX-4 was calculated from c_p ($J\cdot kg^{-1}\cdot K^{-1}$), density, ρ ($kg\cdot m^{-3}$), and thermal diffusivity, α ($m^2\cdot s^{-1}$), viz., $\lambda = c_p\cdot\rho\cdot\alpha$. The c_p and density values were taken from the literature.[7] The c_p values between 1073 K and 1573 K were calculated assuming (i) estimated c_p values and (ii) that enhanced c_p values representing a ΔH^{trans} contribution. Since the thermal diffusivity values are scattered in the high temperature range, the maximum and minimum thermal conductivities were estimated from the thermal diffusivities. The thermal conductivity of the CMSX-4 thus estimated is presented in Figure 4. The thermal conductivity of the CMSX-4 could also be estimated by the Wiedemann−Franz law, viz., $\lambda = L_0\cdot\sigma\cdot T$, where L_0 is the Lorenz number ($2.44\cdot10^{-8}$ $W\Omega K^{-2}$) and σ is the electrical conductivity. The value of the electrical conductivity was taken from ref 8. This calculation result is also presented in Figure 4. From the comparison of the values from the present experimental results ($c_p\cdot\rho\cdot\alpha$) and the

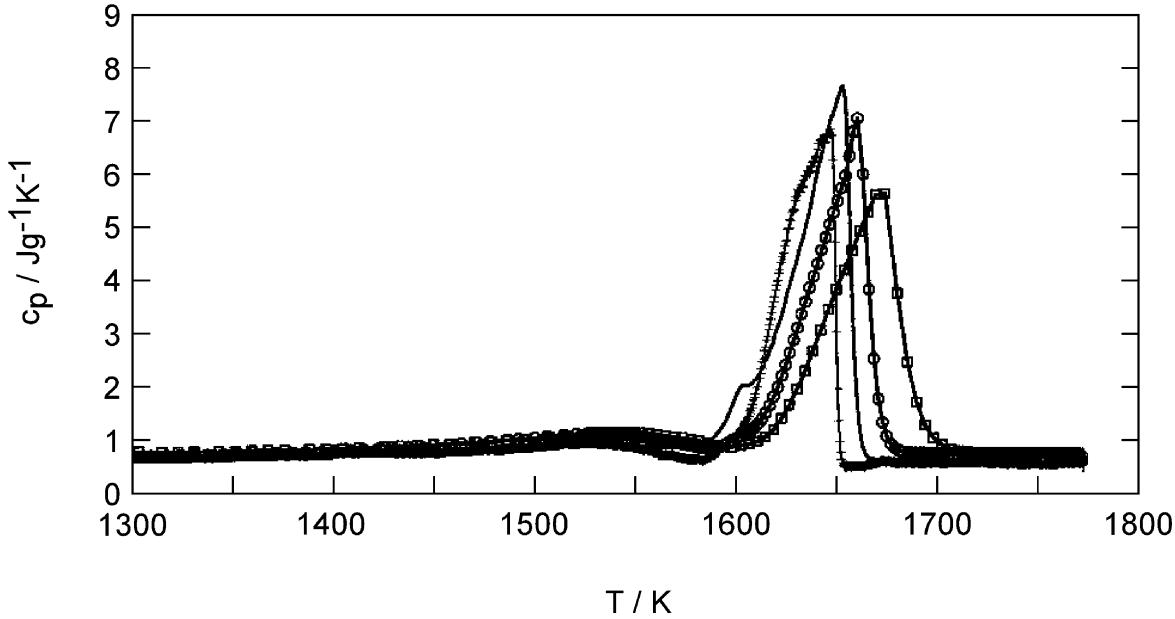

Figure 5. Specific heat capacity of CMSX-4 alloy as a function of temperature, *T*/ K.[9] −□−, 40 K·min^{-1}, 98.60 mg; −○−, 20 K·min^{-1}, 96.30 mg; −, 10 K·min^{-1}, 145.20 mg; and −|− 5 K·min^{-1}, 98.80 mg.

Wiedemann−Franz law, it was found that the contribution of electrons in thermal conduction is likely to be about (60 to 80) % (from the maximum estimation of α) and about (70 to 100) % (from the minimum estimation of α). The contribution of the photon to the thermal conductivity can be described by the following equation

$$\lambda_r = \frac{16}{3}\cdot\sigma_B\cdot n^2\cdot T^3\cdot\alpha_a^{-1} \quad (1)$$

where σ_B is the Stefan−Boltzmann constant; n is the refractive index; and α_a is the absorption coefficient. However in the case of metallic systems, the transmissivity is quite low (= low α_a^{-1} value). Therefore, the contribution of the photon can be ignored in the present system even at high temperatures (= high T^3 value in the equation). Hence the rest of the contribution to the thermal conductivity should be by the phonons.

3.4. DSC Measurements. As can be seen from the calculated phase diagram (Figure 1), there are no phase changes in the system in the temperature range 1100 K to solidus temperature. This is in conformity with the heat capacity measurements as well. Further, there is no information available regarding the impact of structural changes of the alloy on the heat capacity results, such as, for example the dissolution of the γ' phase.

It was found that the apparent c_p value is not strongly affected by the heating rate in the lower temperature range. On the other hand, in the higher temperature range, the differences observed are significant. The apparent c_p value became less with an increase of the heating rate.[6] Chapman also observed similar trends. The figure is reproduced in Figure 5.[9]

In the lower temperature range, the specific heat capacity was also measured with a Perkin-Elmer power compensated DSC by the step heating method which in this temperature range provides the most accurate values of the specific heat capacity. In Figure 6, a comparison between the specific heat capacity values obtained by the step heating method and by a scanning HTDSC is shown. Very good agreement between the specific heat capacity values obtained by different instruments and in different laboratories is obtained. In Figure 7, the specific heat capacity in the solid phase up to a temperature of 1573 K is shown in more detail.

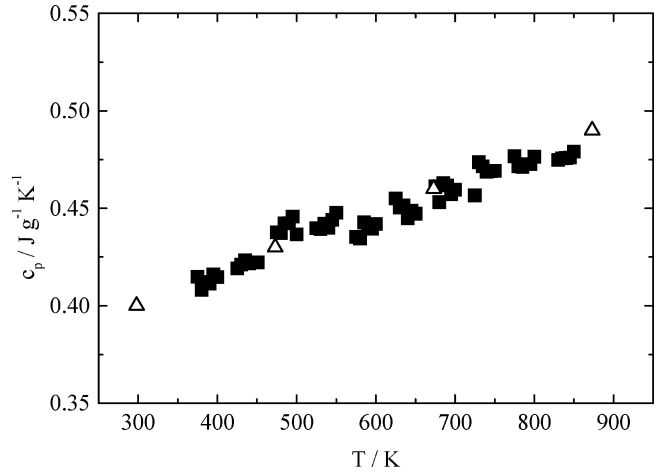

Figure 6. Comparison of the specific heat capacity on CMSX-4 obtained with the power compensated DSC at the University of Ulm (■) and with an HTDSC at NPL (△).

The pronounced increase in the specific heat capacity can not be due to the phonon part alone which should be nearly constant at the Dulong-Petit value of 3R. According to the calculated phase diagram, the pronounced increase in the apparent c_p which corresponds to an endothermal process in the specimen is associated with the dissolution of the γ' phase. The maximum endothermal heat flow is observed at $T = 1519$ K indicating that the dissolution of the γ' phase is nearly finished at this temperature which is about 120 K higher than predicted in the calculated phase diagram. The increase of the final γ' dissolution temperature may be related to the neglect of Ta in the calculated phase diagram or more likely to a kinetic effect related to the Ta atom. Ta is the largest atom and a slow diffusor with different solubilities in the γ/γ' phases. Thus, the presence of Ta atoms could kinetically retard the γ' phase dissolution and concentration equilibration in the γ phase.

In Figure 8, the microstructure of an as-received and of the specimen heated in the HTDSC with $R_H = 20$ K·min^{-1} to $T = 1573$ K is shown. The cooling rate was $R_C \approx 50$ K·min^{-1}. The

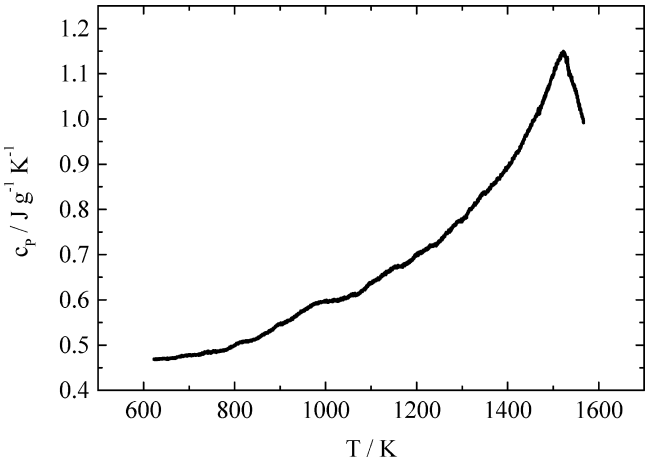

Figure 7. Specific heat capacity of CMSX-4 (as cast) in the solid phase as a function of temperature, *T*/K. Netzsch HTDSC.

microstructure of the specimen heated to 1573 K is coarser than that of the as-received specimen. In the as-delivered part, the γ' phase precipitates to have an average size of 340 nm as compared to an average grain size of 580 nm in the part heated to 1573 K. The phase diagram and the DSC heat flow shown in Figures 1 and 7, respectively, indicate that at $T = 1573$ K the γ' phase has dissolved. The coarser microstructure of the heat treated sample results from reprecipitation of the γ' phase.

It would be interesting to compare the results obtained for apparent heat capacities with those obtained by the Neumann−Kopp rule

$$c_p(A_xB_y) = xc_p(A) + yc_p(B) \quad (2)$$

where $c_p(A_xB_y)$ is the heat capacity of a compound A_xB_y and $c_p(X)$ is the heat capacity of element X.

Such an exercise was carried out for the Ni-base alloy with the following major components: Ni, Co, Cr, Ta, W, Al, Re, and Ti. The c_p value of each element was taken from the literature.[10] Regarding the c_p value of tungsten, the data were taken from ref 11. Tonooka[6] has proposed recommended c_p values of CMSX-4 in the temperature range of $313 < T/K < 1400$

$$c_p = 1.454 + 0.01672T\ [J\cdot(mol\cdot K)^{-1}]\ (313 < T/K < 1400) \quad (3)$$

The above recommended c_p value was obtained by taking the average c_p values of the experimental results from different heating rates. A comparison of the two equations reveals that the experimental c_p values are slightly higher compared to those derived from the Neumann−Kopp rule. This may be attributed to the dissolution of the γ' phase in the wide temperature range during the measurements.

In addition to the heating rate dependency of the apparent c_p values, the peak temperature for the melting process was also found to be different for different heating rates also observed (Figure 5).[9]

The values of the peak temperature for each heating rate, obtained at KTH, are summarized in Table 2 along with literature values.

To analyze the data, the Kissinger method[12,13] was employed. This method is well-known to determine the apparent activation energy, E_a, of the chemical reaction or crystallization. To the knowledge of the present authors, this method has not been applied to the kinetics of the process between solidus temperature and liquidus temperature.

To determine the apparent activation energy of the melting process, the Kissinger method was used in the present work. The DSC measurements were carried out at different heating rates. The heating rate designated as β and the temperature at peak position of the signal, T_p, are presented in Table 2. The $\ln(\beta/T_p^2)$ was plotted against $1/T_p$ (Figure 9). As can be seen from Figure 9, the linear relationship was obtained. From the slope of the lines, the apparent activation energy was calculated based on the Kissinger equation

$$\ln(\beta/T_p^2) = A - E_a/RT_p \quad (4)$$

where A is the constant; E_a is the apparent activation energy; and R is the gas constant. The results are summarized in Table 2.

The Kissinger plots obtained in the present work as well as those calculated using the results of Chapman are in good agreement with each other as can be seen in Figure 9. The values should be corresponding to the activation energy for "melting process" in this system.

The present set of measurements is intended to be of importance in the materials design as the results pertain to samples in the nonequilibrium state, close to the applications. Thus, the results indicate the values of the as-received samples, which is expected to be a measure of the extent of deviation from the thermodynamic equilibrium state. The Thermolab project results corresponding to the measurements of the physical properties of a number of alloys in nonequilibrium state could open up the possibilities of quantifying the extent of deviation from the equilibrium state and eventually even predict the values of the physical properties of these industrial alloys. Such an exercise would be of immense help in material design for newer alloy systems for specific applications.

3.5. Fraction Solid. The fraction solid on cooling is an important parameter in solidification modeling as it determines the rate of enthalpy generation and thus the temperature−time behavior. The fraction solid/liquid is usually determined as the fractional area of the DSC heating and cooling curves for different heating and cooling rates. By default, this approach assumes that the enthalpy of fusion or solidification is independent of the composition. Results for heating and cooling are shown in Figure 10.[14] On cooling, the specimen in the DSC exhibited a variable degree of undercooling which makes a comparison with an industrial production process difficult.

3.6. Enthalpy of Fusion. The enthalpy of fusion was measured with a NETZSCH Jupiter DSC with the typical set up of sample and reference pan. Measurements were performed at a heating rate of 20 $K\cdot min^{-1}$ under flowing argon with a nominal purity better 0.1 ppm. Calibration was performed by first determining the calorimeter sensitivity function with a NBS related sapphire standard. Then the enthalpy of fusion of a Ni-standard of the same mass as the specimen of interest was measured. The calibration factor such obtained, $f_H = \Delta H_{Ni}(st)/\Delta H_{Ni}(m)$, with $\Delta H_{Ni}(m)$ the measured and $\Delta H_{Ni}(st)$ the standard value, was then scaled with the change in the calorimeter sensitivity function, $S(T)$, between the liquidus temperature of CMSX-4, T_l, and the melting temperature of Ni, T_{Ni}. Thus $f_S(T) = S(T_{Ni})/S(T_l)$. The final calibration factor was set as $f_c(T) = f_S(T)f_H$ and thus: $\Delta H_f = f_c(T)\Delta H_f(m)$, with $\Delta H_f(m)$ being the measured enthalpy of fusion of the specimen of interest. The

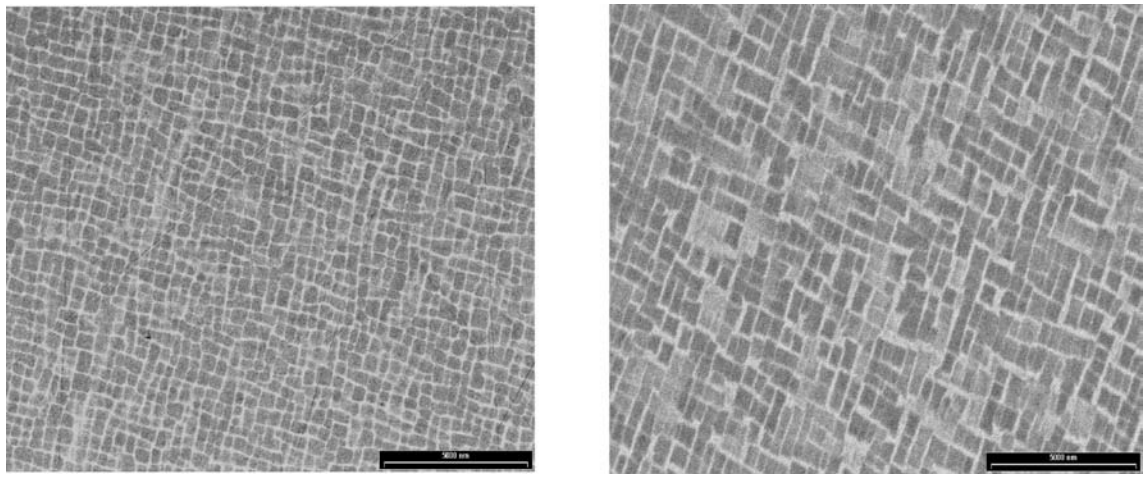

Figure 8. (a) SEM micrograph of an as-delivered specimen. Black bar = 5 μm. (b) SEM micrograph of a specimen heated to T = 1573 K. Black bar = 5 μm.

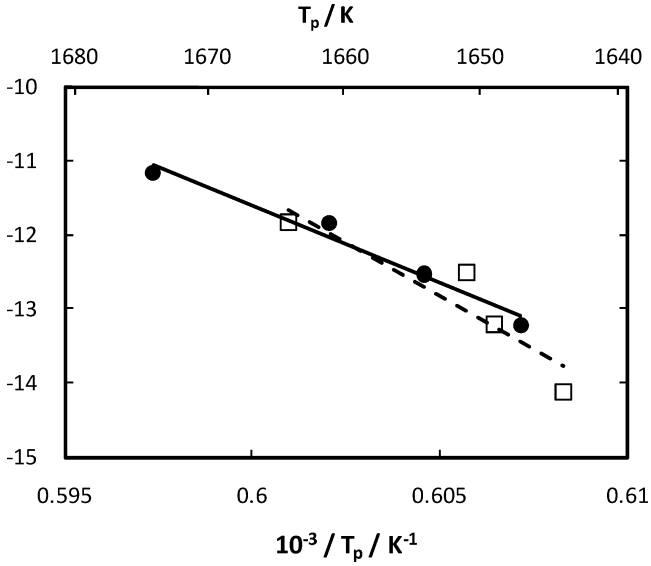

Figure 9. Kissinger plots of the temperature of maximum heat flow as a function of the heating rate during melting. $\ln(\beta/T_p^2)$ against $10^{-3}/T_p/K^{-1}$. −□−, ref ; and −●−, ref 9.

Table 2. Temperature at Peaks and Activation Energy Calculated from the Literature Data

heating rate	temperature at peak		activation energy
β/(K·min^{-1})	T_p/K	refs	E_a/(kJ·mol^{-1})
5	1647	ref 9	1731
10	1654		
20	1661		
40	1674		
2	1644	ref 6	2406
5	1649		
10	1651		
20	1664		

final result representing an average of values obtained in three participating laboratories is listed in Table 3. The liquidus temperature was obtained from an extrapolation of the apparent liquidus temperatures from heating rate dependent measurements to zero heating rate. The solidus temperatue was obtained from the onset of melting measured with a heating rate of 5 K·min^{-1} as shown in Figure 5. As such we obtain T_{sol} = (1594 ± 6) K and T_{liq} = (1654 ± 5) K.

3.7. Specific Heat Capacity in the Liquid Phase. The specific heat capacity in the liquid phase is difficult to measure. First,

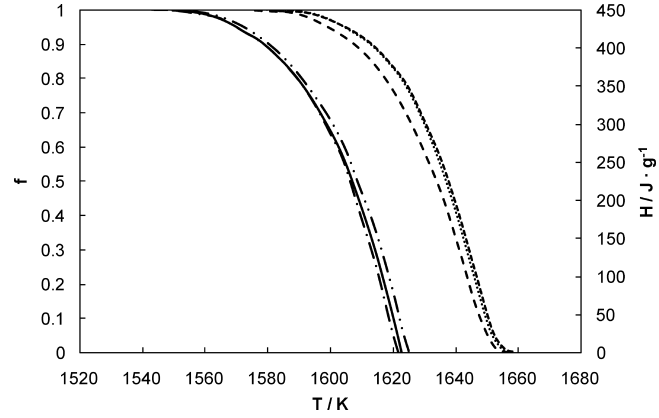

Figure 10. Fraction solid, f, as a function of temperature on heating and on cooling. R_H = 10 K·min^{-1}, and corresponding enthalpy, H. CMSX4 PHB (mass = 131.8 mg) Run at 10 K·min^{-1}. — •• —, Fraction Solid PHB first cool, H_f = 202.5 J·g^{-1} [208.9]; —, Fraction Solid PHB second cool, H_f = 206.1 J·g^{-1} [210.9]; -•-•-, Fraction Solid PHB third cool, H_f = 206.2 J·g^{-1} [210.3]; - - - -, Fraction Solid PHB first heat, H_f = 193.5 J·g^{-1} [194.7]; ••••, Fraction Solid PHB second heat, H_f = 193.1 J·g^{-1} [194.0]; and — — —, Fraction Solid PHB third heat, H_f = 196.2 J·g^{-1} [196.1].

Table 3. Enthalpy of Fusion/Solidification of CMSX-4

	H_f/(J·g^{-1})
heating	231 ± 13
cooling	227 ± 20

Table 4. Specific Heat Capacity in the Liquid Phase of CMSX-4

T/K	1703	1723	1753	1773	1793	1813
c_p/(J·K^{-1}·g^{-1})	0.74	0.78	0.78	0.77	0.76	0.75

there is the potential of chemical or dissolution reactions between the liquid sample and the container. Second, the change in surface and contact area of the specimen upon melting which determine heat loss and heat flow to the sensing device will affect the calibration relative to a stable standard such as sapphire. As an example, if the liquid sample would not wet the container the rate of heat flow into the sample would be strongly diminished while heat loss from the surface would be increased resulting in an apparent increase in c_p relative to a stable standard and a pronounced heating rate dependence of c_p. As it turned out, pure Ni had the same wetting properties as CMSX-4. As such, the specific heat capacity of Ni including +50 K into the liquid phase was measured in the usual way with baseline, sapphire, and sample run. The specific heat capacity of Ni in the liquid phase such obtained was then

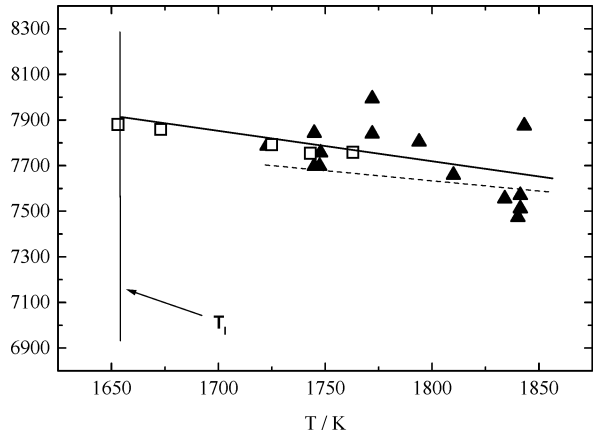

Figure 11. Density, ρ/kg·m^{-3}, of CMSX-4 as a function of temperature, T/K, measured on electromagnetically levitated specimen (▲) and on sessile drop (□). Solid line, fit to experimental data; dashed line, calculated values by K. Mills.

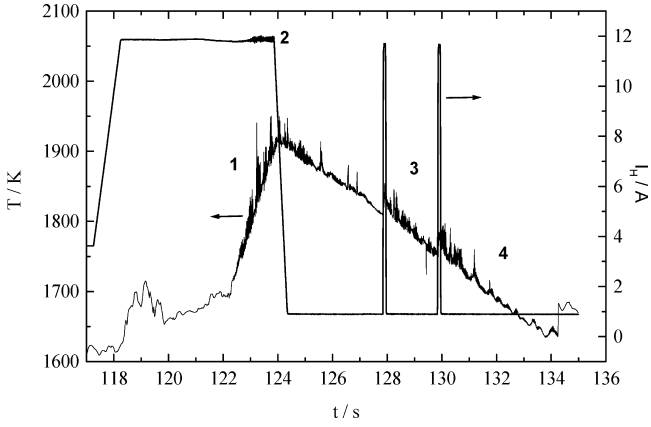

Figure 12. Temperature−time and rf-heater current−time profile during processing of a CMSX-4 specimen in the microgravity phase of a parabola. Temperature is shown on the left-hand ordinate, indicated by an arrow. The heater oscillating circuit current is shown on the right-hand ordinate indicated by an arrow. 1, Melting and heating into the liquid phase; 2, turning off of the heater nearly force free cooling; 3, application of pulses for the excitation of surface oscillations; 4, further cooling to solidification.

corrected with the tabulated values for liquid Ni from which a correction factor $f_{Cp} = C_{Ni}(st)/C_{Ni}(m)$ with $C_{Ni}(st)$ and $C_{Ni}(m)$ being the reference and measured specific heat capacity values, respectively. Then the heat capacity of the CMSX-4 sample of equal mass was measured in the same way. The specific heat capacity in the liquid phase, $c_p(liq)$, was then obtained from

$$c_p(liq) = f_{Cp} c_p(m) \quad (5)$$

with $c_p(m)$ being the measured heat capacity. It was assumed that the correction factor is temperature independent. f_{Cp} was in the range $f_{Cp} = 1.36 \pm 0.10$ showing that considerable inaccuracy is present in this approach. The change in calorimeter sensitivity is already considered because the c_p measurements for Ni and CMSX-4 are referenced via the sapphire run to the calorimeter sensitivity in the respective temperature. The results such obtained are summarized in Table 4.

The error in the specific heat capacity orignates primarily from the calibration factor f_{Cp} for the measurement in the liquid phase. This factor includes the change in the heat flow conditions from a solid calibration standard to a measurement in the liquid phase. In the solid phase, the c_p values obtained with the NETZSCH high-temperature DSC are accurate within 3 % when compared with a standard like pure Fe. As such, the error of the specific heat capacity in the liquid phase is estimated as ± 12 %.

3.8. Density in the Liquid Phase. The density in the liquid phase represents another thermophysical property necessary for casting and solidification modeling regarding convective heat transport and the prediction of structure defects such as a freckle. The density in the liquid phase was measured by optical methods on an electromagnetically levitated specimen and by the sessile drop technique.[15] Results are shown in Figure 11. Measurements were performed under a high-purity Ar atmosphere. Results from both methods are shown in Figure 11. The data can be very well fitted by a linear function. Where the temperature ranges overlap, results obtained from both experiments agree to better than 1.5 %.

Electromagnetic levitation:

$$\rho(T) = 7781 - 0.411(T - 1653\ \mathrm{K})\ \mathrm{in\ kg{\cdot}m^{-3}} \quad (6)$$

Sessile drop technique:

$$\rho(T) = 7881 - 0.137(T - 1653\ \mathrm{K})\ \mathrm{in\ kg{\cdot}m^{-3}} \quad (7)$$

Combination of the two sets of data, 1653 K to 1843 K:

$$\rho(T) = 7876.4 - 1.231(T - 1653\ \mathrm{K})\ \mathrm{in\ kg{\cdot}m^{-3}} \quad (8)$$

K. C. Mills:[16]

$$\rho(T) = 7754 - 0.9(T - 1653\ \mathrm{K})\ \mathrm{in\ kg{\cdot}m^{-3}} \quad (9)$$

The deviation between the measured data and the calculated values is lower than 1.5 %.

3.9. Surface Tension and Viscosity. The surface tension and in particular the viscosity are relevant for fluid flow calculations. The surface tension is often measured by the sessile drop method and the viscosity by the rotating or oscillating cup method. Containerless methods offer an alternative approach in particular for high melting point reactive liquids such as, e.g., Ti-alloys. While the surface tension can be measured by the oscillating drop method in an electromagnetic levitation device in ground-based laboratory, this is not the case for the viscosity. For the evaluation of the surface tension from the surface oscillation frequency, a correction method has been developed[17] to account for the additional surface force exerted by the levitation field. This correction was quantitatively verified in a microgravity experiment where the magnetic forces required to position a metallic specimen are much reduced.[18] A similar correction is not available for the viscosity. The turbulent fluid flow induced by the strong magnetic forces required for levitation under normal gravity conditions affects the damping of the surface oscillations in a way which is difficult to quantify. As such, reduced gravity conditions are required for the application of the oscillating drop method for viscosity measurements.

Parabolic flights have been used extensively in the Thermo-Lab project for surface tension and viscosity measurements of industrial alloys.[19] Parabolic flights provide about 20 s of reduced gravity. This time is sufficient for melting, heating into the liquid phase, and cooling a specimen to solidification. The sample is heated by a radio frequency (rf) electromagnetic dipole field and positioned by a rf quadrupole field. In the free cooling

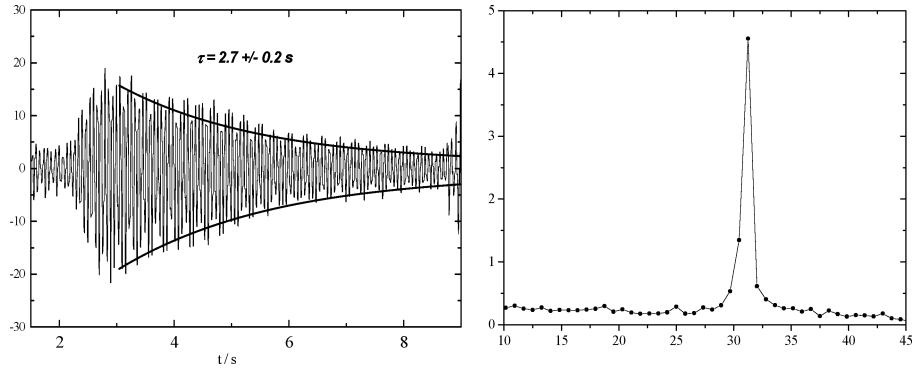

Figure 13. (a) Variation of the sample diameter (X-radius Variation, r_x/Pixel) as a function of time, t/s, in the direction perpendicular to the dipole field axis following pulse excitation with the heating field. (b) Fourier spectrum of a 0.64 s time slice of the sample diameter variation shown in Figure 13a. Amplitude against frequency f/Hz.

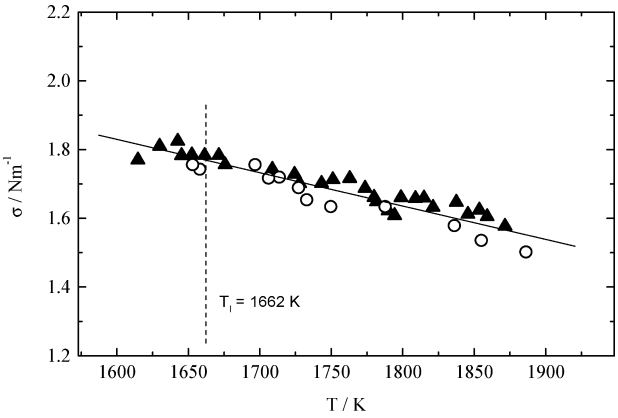

Figure 14. Surface tension, σ/N·m^{-1}, of the "low oxygen" CMSX-4 specimen as a function temperature, T/K; data collected from two parabolas.

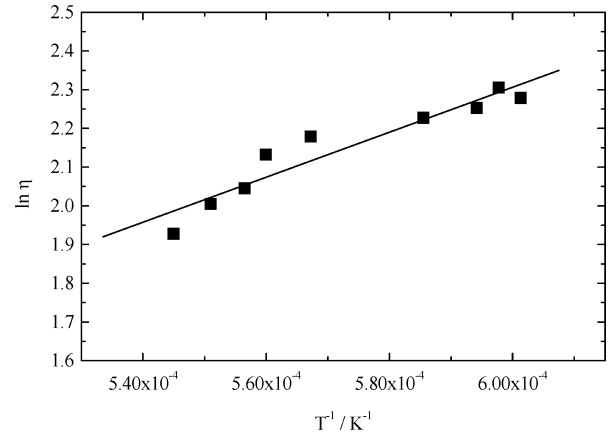

Figure 15. Arrhenius plot of the viscosity of the low oxygen specimen. Natural logarithm of the viscosity, η, against inverse temperature.

phase with the heating field turned off, magnetic field pulses are applied for the excitation of surface oscillations. The specimen shape is recorded by two cameras. For the CMSX-4 experiments, 100 Hz frame rate analogue cameras were used. In the meanwhile, these were replaced by two 200 Hz framerate digital cameras. A typical temperature−time profile with a CMSX-4 sample from the parabolic flight experiments is shown in Figure 12.

From the frequency, ν, and the damping time constant, Γ, of the surface oscillations, the surface tension, σ, and the viscosity, η, can be evaluated according to

$$\sigma = \frac{3}{8}\cdot\pi\cdot\nu^2\cdot M \tag{10}$$

and

$$\eta = \frac{3}{20\pi}\cdot\frac{M}{r}\cdot\Gamma^{-1} \tag{11}$$

with M and r being the mass radius of the specimen, respectively. In Figure 13a and b, the time variation of the change in specimen radius and the Fourier transformation of a 0.64 s time slice are shown, respectively. The surface tension as a function of temperature is shown in Figure 14. The data can be well represented by a linear fit according to

$$\sigma = 1.79 - 9.09\cdot10^{-4}\,(T - 1655\ \mathrm{K})Nm^{-1} \tag{12}$$

The values shown in Figure 14 do not agree with the results by the drop-weight and oscillating-drop methods by Vinet et al.[20] The inconsistency needs to be investigated further. The precision of the frequency determination for an individual data point as shown in Figure 14 is estimated as ± 2 % which translates into a precision of ± 4 % in the surface tension values. The scatter of the surface tension values between different parabolas can be caused by slight changes in environmental conditions which are difficult to control. As such, an error of ± 6 % in the surface tension value at the liquidus temperature appears appropriate.

An Arrhenius plot of the viscosity as a function of temperature is shown in Figure 15. From these data, the activation energy, ΔE_a, for viscous flow and the prefactor, η_o, according to

$$\ln\eta(T) = \ln\eta_o + \frac{\Delta E_a}{R}\cdot\frac{1}{T} \tag{13}$$

with R being the universal gas constant, are obtained as

$$\eta_o = 0.31\ \mathrm{mPa\cdot s}$$

$$\Delta E_a = 0.42\ \mathrm{eV/atom}$$

The viscosity at the liquidus temperature $T_l = 1655$ K was obtained as 10.3 mPa·s. This number is about 20 % higher than a value which has been measured by the oscillating cup method in the same project. The activation energy and prefactor are typical for Ni-based alloys. Moreover, in the parabolic flight

experiment two CMSX-4 specimen with different initial oxygen content were investigated. The oxygen content was determined by the LECO hot gas extraction method on samples from similar prepared batches as (0.0043 and 0.0340) mass %. The viscosity of the high oxygen specimen was about 20 % higher than that of the low oxygen specimen, while the video recordings did not indicate the presence of surface oxide precipitates. Up to now, there are no systematic investigations of the effect of dissolved oxygen on the viscosity available. Some scattered results indicate indeed an increase in the viscosity, e.g., for Al, for specimen with a higher oxygen content.[21] Besides the scientific interest, these findings are also relevant for the accurate measurement of the viscosity of industrial alloys and may well be responsible for some of the scatter in viscosity values reported in the literature.

4. Conclusions

Thermal diffusivity and specific heat capacity of CMSX-4 alloy were measured as a function of temperature. The temperature dependency of the thermal diffusivity was discussed based on the calculated phase diagram as well as microstructure study. The results could be explained reasonably. The thermal conductivity was calculated from experimental results as well as the Wiedemann−Franz law. It was found that the contribution of electrons in thermal conduction is likely to be about (60 to 100) %. The c_p (DSC) values were compared with the calculated value from the Neumann−Kopp rule. Further, the heating rate dependency on the DSC peak temperature position was discussed.

Literature Cited

(1) Ormerod, J.; Taylor, R.; Edward, J. Thermal diffusivity of cast irons. *Metal Technol.* **1978**, 109–113.

(2) Brooks, R. F.; Day, A. P.; Mills, K. C.; Quested, P. N. Physical property measurements for the mathematical modeling of fluid flow in solidification processes. *Int. J. Thermophys.* **1997**, *18*, 471–480.

(3) Taylor, R. E. Heat-pulse thermal diffusivity measurements. *High Temp.-High Press.* **1979**, *11*, 43–58.

(4) Schriempf, J. T. Laser flash techniques for determining thermal diffusivity of liquid metals at elevated temperatures: Applications to mercury and aluminum. *High Temp.-High Press.* **1972**, *4*, 411–416.

(5) Abas, R. A.; Hayashi, M.; Seetharaman, S. Thermal diffusivity measurements of CMSX-4 alloy by the laser-flash method. *Int. J. Thermophys.* **2007**, *28*, 109–122.

(6) Tonooka, Y. *Royal Institute of Technology, Sweden, Department of Materials Science and Engineering, Internal reporting*, ISRN: KTH/MSE−05/10−SE+THMETU/EX, **2005**.

(7) Mills, K. C.; *Recommended Values of Thermophysical properties for Selected Commercial Alloys*; Woodhead Publishing Limited: Cambridge, 2002; pp 173.

(8) Roebuck, B.; Cox, D.; Reed, R. The temperature dependence of γ' volume fraction in a Ni-based single crystal superalloy from resistivity measurements. *Scripta Mater.* **2001**, *44*, 917–921.

(9) Chapman, L. A. *J. Mater. Sci.* Application of high temperature DSC technique to nickel based superalloys. **2004**, *39*, 7229–7236.

(10) Kubaschewski, O.; Alcock, C. B. *Metallurgical Thermochemistry*, 5th ed. (Revised and Enlarged); Pergamon Press: Oxford, 1979.

(11) Chase, M. W., Jr.; Davies, C. A.; Downey, J. R., Jr.; Frurlp, D. J.; McDonald, R. A.; Syverud, A. N. *JANAF Thermochemical Tables Third Edition Part II, Cr-Zr*; American Chemical Society and the American Institute of Physics for the National Bureau of Standards, 1985.

(12) Kissinger, H. E. Variation of peak temperature with heating rate in differential thermal analysis. *J. Res. Natl. Bur. Stand.* **1956**, *57*, 217–221.

(13) Kissinger, H. E. Reaction Kinetics in Differential Thermal Analysis. *Anal. Chem.* **1957**, *29*, 1702–1706.

(14) THERMOLAB Project, Physical Science Unit, Directorate of Human Spaceflight, Microgravity and Exploration, European Space Agency - ESA/ESTEC (HME-GA) Keplerlaan 1, 2201 AZ Noordwijk, Netherlands, 2001.

(15) Brooks, R.; Egry, I.; Ricci, E.; Seetharaman, S.; Wunderlich, R. Thermophysical property measurements of high-temperature liquid metallic alloys–state of the art. *High Temp. Mater. Process.* **2006**, *25*, 303–322.

(16) Mills, K. C. NPL, Recommended values of thermophysical properties for selected commercial alloys, ASM International, ISBN 0-87170-753-5, 2002; p 167.

(17) Cummings, D. L.; Blackburn, D. A. Oscillations of magnetically levitated aspherical droplets. *J. Fluid Mech.* **1991**, *224*, 395–416.

(18) Egry, I.; Lohoefer, G.; Jacobs, G. Surface tension of liquid metals: Results from measurements on ground and in space. *Phys. Rev. Lett.* **1995**, *75*, 4043–4046.

(19) Higuchi, K.; Fecht, H.-J.; Wunderlich, R. K. Surface tension and viscosity of the Ni-based superalloy CMSX-4 measured by the oscillating drop method in parabolic flight experiments. *Adv. Eng. Mater.* **2007**, *9*, 349–354.

(20) Vinet, B.; Schneider, S.; Garandet, J. P.; Marie, B.; Drevet, B.; Egry, I. Surface tension measurements on CMSX-4 superalloy by the drop-weight and oscillating-drop methods. *Int. J. Thermophys.* **2004**, *25*, 1889–1903.

(21) Dinsdale, A. T.; Quested, P. N. The viscosity of aluminum and its alloys–A review of data and models. *J. Mater. Sci.* **2004**, *39*, 7221–7228.

Received for review January 30, 2009. Accepted March 12, 2009. This work was performed as part of the ThermoLab project. The financial support received from European Space Agency is gratefully acknowledged. R. K. Wunderlich and H.-J. Fecht would like to acknowledge support from the German Space Agency, DLR, under contract 50WM0540 and from the European Space Agency MAP programme (Microgravity Application Support Programme) under contract AO-99-022 (14306/01/NL/SH).

JE900132M